# Journal of Materials Chemistry A

Accepted Manuscript


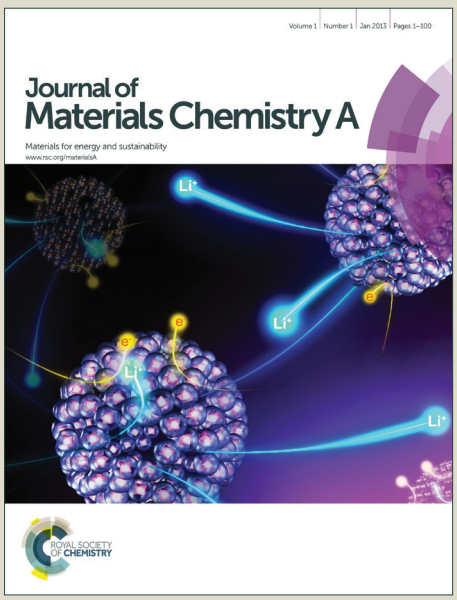





ROYAL SOCIETY OF CHEMISTRY

www.rsc.org/materialsA

Journal Name

RSCPublishing

ARTICLE

# CN Foam Loaded with Few-layer Graphene Nanosheets for High-performance Supercapacitor Electrode

Cite this: DOI: 10.1039/x0xx00000x

Guoxing Zhu,[a,c,*] Chunyan Xi,[a] Yuanjun Liu,[b] Jun Zhu,[a] and Xiaoping Shen[a,*]

Received 00th January 2012,
Accepted 00th January 2012

DOI: 10.1039/x0xx00000x

www.rsc.org/

Three-dimensional porous carbon-based foams have recently attracted increasing interest owing to their exciting potential in various fields. Herein, hierarchical porous monoliths, CN foam loaded with free few-layer graphene nanosheets, have been prepared. In this method, graphene oxide sheets were firstly loaded on the usual melamine foam that was selected as raw material for CN framework. With a following annealing process in $N_2$ atmosphere, melamine foam was transferred into CN foam; at the same time, graphene oxide sheets were transferred into reduced graphene oxide, forming reduced graphene oxide-CN composite. The loading density of graphene on CN framework can be tuned by the dosage of graphene oxide. The obtained composite monoliths exhibit excellent cycling performance and good rate capacity when used as pseudocapacitive electrode materials. At current density of 0.5 and 10 A/g, the optimized electrode exhibits areal specific capacitance of 1067 and 463 mF/cm$^2$ with excellent cycling stability. The excellent property can be attributed to the unique macropore structures that endow sufficient space available to interact with the electrolytes, and the pseudocapacitive contribution originated from the nitrogen and oxygen composition. This facile synthesis strategy and the good electrochemical properties suggest the synthesized CN-graphene composites are promising materials for supercapacitor application.

## Introduction

As a kind of promising energy device with features of high power density, fast charge/discharge rates, and long cycle life, supercapacitors have attracted a great deal of attention from both industry and academia.[1-2] The key part of a supercapacitor is the electrode material, which predominantly depends the charge storage performance.[3-4]

Owing to the intrinsic advantages such as low cost, lightweight, high operational stability, and excellent electric conductivity, carbon is the mostly used electrode material for supercapacitors. Carbon-based materials are not only used in electrochemical double layer capacitors for charge storage, but also employed in pseudocapacitors for improving the conductivity.[5-10] During the past several years, various carbon materials, including activated carbon,[11-13] carbon nanotubes,[14-16] and graphene,[17-20] have been investigated for use in supercapacitors.

For a carbon-based electrode, it has been confirmed that porous structure with bigger specific surface area is preferred for excellent capacitance performances.[21-23] While, porous structure is not still enough. High electric conductivity and suitable pore size are also required. Although porous structure will increase their specific surface area, smaller pores will restrict electrolyte ion diffusion during the charge/discharge process.[21] In this situation, their surface cannot be effectively utilized and so cannot contribute to charge storage.[24, 25] Thus, fabricating macro-porously structured carbon with high accessible surface area and excellent electrical conductivity will be beneficial to its application as supercapacitor electrode. Up to date, there are some reports about the preparation and application of macroporous carbon-based materials as capacitor electrodes.[26-30] For example, Feng *et al* has fabricated a three-dimensional hierarchical graphene/polypyrrole aerogel using graphene oxide (GO) and one-dimensional hollow polypyrrole nanotubes as feedstocks.[29] With a polystyrene colloidal particle template method, Choi *et al* has prepared a three-dimensional macroporous carbon structure loaded with $MnO_2$.[31] The obtained composite shows enhanced charge storage performance.

Since Hulicova *et al* prepared nitrogen-doped carbon in 2005 by carbonization of melamine with the assistance of mica,[32, 33] melamine-based polymer such as melamine formaldehyde resine were often selected as raw or assistant

materials for functional carbon materials.[34-36] Carbonization of various organic precursors containing melamine can synthesize nitrogen-doped carbon materials, which often have a highly porous nanometer-sized honeycomb structure and show a high specie surface area.[37-41] It was demonstrated the melamine-derived carbon show better electrical chemical performances owing to nitrogen doping.

Herein, with melamine foam as raw materials, we demonstrate a robust and rapid method to prepare macro-porous CN-reduced graphene oxide (CN-RGO) composite monoliths with a high porosity, in which few-layer RGO nanosheets are uniformly loaded on the CN framework. The loading density of RGO can be easily tuned by the dosage of graphite oxide. The unique structure of CN-RGO composite possesses several major advantages for supercapacitor application: (1) the ultrathin sheet-like RGO is free and not stacked owing to the presence of CN framework, which ensures high accessible specific surface area and so is beneficial to accumulating a large amount of charges; (2) the composite monolith has macro-porous structure, which is favorable for the quick electrolyte ion diffusion during the charge/discharge process; (3) the coexistence of CN framework and high conductive RGO contributes to high electrical conductivity and ensures fast electron transfer process; and (4) the CN framework, different from pure carbon network, will provide pseudocapacitor contribution owing to the presence of nitrogen element with high content. The composite foams show high specific capacitances of ~162 F/g and areal capacitor of 1067 mF/cm$^2$ at scan rates of 0.5 A/g and excellent cycle life with ~95% specific capacitance retained after 1,000 cycle tests. The excellent capacitance property could be attributed to the unique structure and the presence of nitrogen and oxygen composition.

## Experimental Section

### Synthesis of the CN-RGO composites

Natural flake graphite with a particle size of 150 μm (99.9% purity) was purchased from Qingdao Guyu Graphite Co., Ltd. Melamine foam was purchased from Beijing Kelin Corp. All other chemicals used in this research are of analytical grade and used without further purification. Graphite oxide was prepared by a modified Hummers' method.[42]

In a typical synthesis process for CN-RGO composites, a certain amount of graphite oxide was dispersed into 30 mL of distilled water. With the assistance of strong ultrasonication for about 1 h, a homogeneous graphene oxide (GO) dispersion was obtained. A piece of melamine foam with size of 2 × 2 × 2 cm$^3$ was then fully immersed into the dispersion, followed by ultrasonication for about 10 min to make it be fully soaked. Then, the melamine foam was carefully taken out from the dispersion and dried naturally at room temperature. With this process, GO sheets were loaded on the melamine foam framework. After that, the composite foam was then annealed in $N_2$ atmosphere at 300 °C for 30 min. Dark black CN-RGO monolith was obtained, which can be easily cut into various shapes and sizes. With different GO feeding amounts such as 6, 30, 60 and 90 mg, CN-RGO monoliths with different RGO loading densities were obtained. The corresponding composites are designated as CN-RGO-6, CN-RGO-30, CN-RGO-60, and CN-RGO-90, respectively.

In addition, with other conditions similar to that of CN-RGO-90 product, another two CN-RGO monoliths were obtained for comparison by changing the calcination temperature to 500 °C and 750 °C, which were donated as CN-RGO-90/500 and CN-RGO-90/750, respectively. Moreover, pristine CN foam and pure RGO were also prepared by directly annealing of melamine foam or graphene oxide in $N_2$ atmosphere at 300-750 °C for 30 min.

### Characterization

The morphology and microstructure analyses of the products were conducted on a Hitachi S-4800 field emission scanning electron microscope (FE-SEM) and a JEOL-2010 transmission electron microscope (TEM). The Fourier transform infrared spectra (FTIR) were recorded on a Nicolet Nexus 470 FTIR spectrophotometer by using KBr disk. The X-ray photoelectron spectrum (XPS) was detected by X-ray photoelectron spectroscopy (Thermo ESCALAB 250) with Al Kα (hν = 1486.6 eV) X-ray radiation source. The spectra were calibrated by C 1s peak (284.6 eV). The Raman spectrum was recorded on a JY HR-800 Raman spectrometer with a 453 nm laser excitation. Elemental analysis of carbon, hydrogen, and nitrogen was conducted on a FLASH1112A Element analyzer. Atomic force microscope (AFM) image was collected on an NT-MDT atomic force microscopy (Russia).

### Electrochemical test

For fabrication of CN-RGO electrodes used in capacitors, a piece of nickel foam (with an area of 1.0 × 1.0 cm$^2$, thickness: 1.0 mm, and pore density: 110 PPI) was carefully washed in sequence with ethanol, acetone, and water to remove contaminants on the surface. Then, a thin CN-RGO sheet (with thickness of ~ 0.5 mm) was cut from the prepared composites with a size of ~1.0 × 0.5 cm$^2$. Subsequently, 30 μL of binder (polyvinylidene fluoride dispersed in water with concentration of 10 mg/mL) was coated on the surface of the cleaned nickel foam. The thin CN-RGO piece was then gently pressed on it. Finally, the obtained electrode was dried at 45 °C for 24 h in a vacuum oven.

The cyclic voltammetry (CV) investigation was carried out at room temperature on a CHI 760D electrochemical workstation (Shanghai, Chenghua Co.) in a three-electrode system with a KOH electrolyte solution (3 M). Cyclic voltammetry experiments were performed at various scan rates of 5, 10, 20, 40 and 80 mV/s. The as-prepared CN-RGO/nickel foam electrode, a Pt foil, and a saturated calomel electrode (SCE) were used as the working electrode, counter electrode, and reference electrode, respectively. The mass loading of the active material is carefully weighed on a Beijing sartorius Balance (max 120 g; d = 0.1 mg). It was determined to be about 4.6 mg/cm$^2$ with account of the CN-RGO sample and the



 

binder. The galvanostatic charge-discharge tests were also performed at room temperature on the CHI 760D electrochemical workstation with the same three electrode system.

## Results and discussion

The preparation procedure of CN-RGO composite foam is illustrated in Fig. 1. Common melamine foam was selected as the raw material for CN framework. GO sheets were firstly loaded on the melamine foam network through a simple immersion route. After that, the composite monolith was annealed in $N_2$ atmosphere to transfer the melamine foam into CN network; at the same time, GO sheets were also transferred into reduced graphene oxide with a well-known thermal reduction procedure. No any modification process is involved in the preparation. Different from the previous report of pure carbon foam obtained from melamine sponge for oil-water separation material, the annealing temperature used here is much lower (300 °C in contrast to 800 °C in the report[41]). It is believed that the lower annealing temperature is responsible for the formation of CN foam.[32,33] Noted that the obtained pristine CN foam is hydrophobic. After loaded with reduced graphene oxide, the monolith is hydrophilic. In addition, after loaded by RGO, the electrical conductivity of the foam is obviously improved (Fig. SI-1, see Supplementary Information). The hydrophilic surface and the improved conductivity is favorable for its application as electrochemical electrode materials.

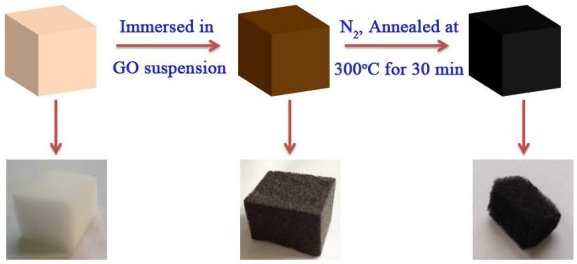


**Fig. 1** The preparation procedure of CN-RGO composite foam.

We firstly determined the composition of the obtained CN-RGO products through element analysis. The pristine CN monolith obtained with 300 °C calcination demonstrates high content of carbon ($_{wt.}$ 41.5%) and nitrogen ($_{wt.}$ 50.3 %) with composition of $CN_{1.04}O_{0.09}$. It should be noted that the composition of pristine CN monolith is highly influenced by annealing temperature. Higher annealing temperature will cause lower nitrogen content (Table SI-1, see Supplementary Information). On the other hand, it is well known that annealing of graphene oxide will cause deoxygen process, inducing reduction of graphene oxide. With 300 °C annealing, graphene oxide with composition of $CO_{0.92}$ was transferred into $CO_{0.009}$. When annealing temperature of 500 °C or 700 °C was selected, $CO_{0.004}$ or $CO_{0.002}$ was obtained, respectively. (Table SI-1, see Supplementary Information). This result suggests that with annealing at 300 °C major oxygen in graphene oxide can be removed; that is, the graphene oxide is partially reduced during the annealing process.[43-45]

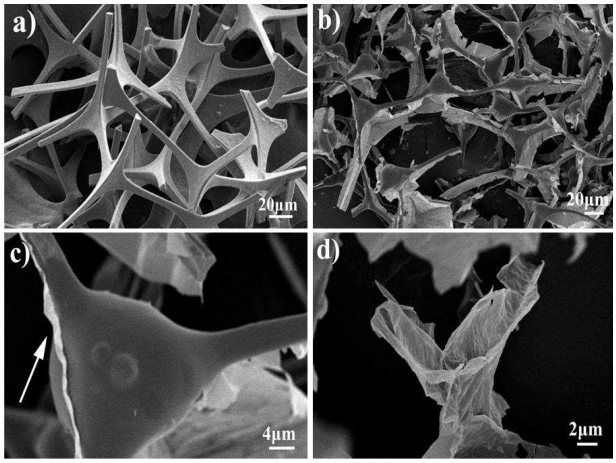


**Fig. 2** SEM images of a) CN foam and b-d) CN foam loaded with RGO (sample CN-RGO-90).

If melamine foam has been loaded with graphene oxide, the final product after annealing shows relatively high oxygen content but relatively low nitrogen content than the pristine CN monolith. The products of CN-RGO-6, CN-RGO-30, CN-RGO-60, and CN-RGO-90 have composition of $CN_{1.01}O_{0.14}$, $CN_{1.05}O_{0.16}$, $CN_{0.79}O_{0.22}$, and $CN_{0.61}O_{0.26}$, respectively. This result suggests that oxygen composition in the composites is mainly contributed from the graphene oxide, while nitrogen is originated from melamine sponge. As shown in Table SI-1 (Table SI-1, see Supplementary Information), similar to that of pristine CN monolith, annealing temperature also has a big influence on the composition of CN-RGO composites. Increasing annealing temperature will cause the decrease of nitrogen and oxygen content (that is, C:O/N ratio increasing) in the final composites. This is consistent with the thermal reduction result of graphene oxide.

This method is effective for loading RGO on the CN foam framework. As shown in Fig. 2a, without RGO, pristine three-dimensional CN foam exhibits a well-defined macroporous structure with pore diameters of 20-100 μm. The frameworks have smooth surface. For the product of composite CN-RGO foam, it can be clearly seen that sheet-like RGO are attached on the framework of CN foam, forming a unique composite structure (Fig. 2b-d). The enlarged SEM image reveals the featured wrinkles of graphene sheets (Fig. 2c, d). It is proposed that graphene nanosheets were loaded on the CN framework with weak interactions but not with covalent graft. Owing to the presence of CN framework, almost all of the RGO nanosheets show free-standing state. In contrast, RGO nanosheets are often stacked in usual RGO powder. This free-standing state makes them have big accessible surface area, which is highly preferred when used as electrode materials. The loading density of graphene on CN framework can be easily tuned by changing

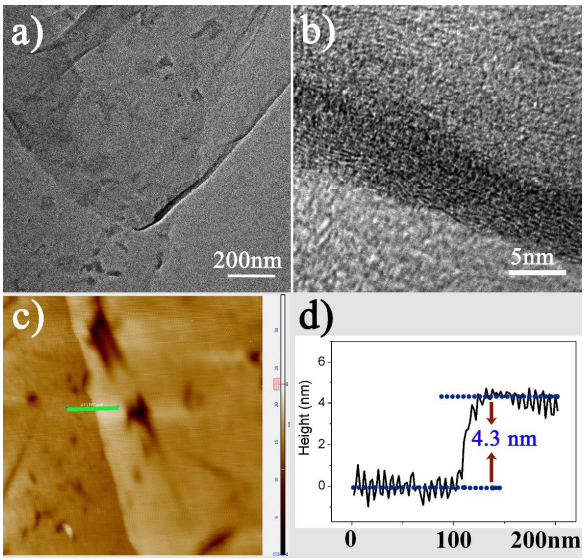


**Fig. 3** a, b) TEM and c) AFM images of CN-RGO composites (sample CN-RGO-90). d) the height profile corresponding to the line in c).

GO concentration. With lower GO concentration, the CN foam is loaded with less amount of RGO.

To determine the thickness of RGO nanosheets loaded on CN framework, the CN-RGO composite was cut into small pieces. With vigorously stirring and strong ultrasonic dispersing, TEM and AFM analysis was then conducted. Fig. 3a, b shows the corresponding TEM images, illustrating sheet-like microstructures, which is typical for RGO. From the curled part of the nanosheet (Fig. 3b), the thickness was estimated to be about 5 nm, suggesting that the nanosheet contains < 10 carbon atomic layers.[46] AFM is a mostly used technique to measure thickness for a sheet-like structure. As shown in Fig. 3c, d, the AFM images give a value of ~4.3 nm for the thickness of the prepared graphene, which is consistent with the TEM observation. These results suggest that the carbon nanosheets loaded on the CN framework is actually few-layer graphene with layer numbers less than ten.

Fig. 4 shows the FT-IR spectra of the obtained CN-RGO composites. At lower wavenumber region, the CN-RGO products show quite similar peaks as that of pristine CN foam. The characteristic absorption peak at 804 $cm^{-1}$ is attributed to out-of plane bending modes of C-N heterocycles.[47] The stretching vibration of C-N bond is observed at 1370 $cm^{-1}$. The band at 1608 $cm^{-1}$ corresponds to the C=C stretching vibration. At higher wavenumber region, the CN-RGO products show a wide absorbance at 3402 $cm^{-1}$, which can be attributed to the residual -OH groups on RGO. It should be noted that many oxygen-containing groups including C=O (at 1733 $cm^{-1}$) disappear if comparing the IR spectra of CN-RGO composites with the original graphite oxide (Fig. SI-2, see Supplementary Information). This indicates that during the annealing process, GO has been partially reduced, which is consistent with the result of elemental analysis.

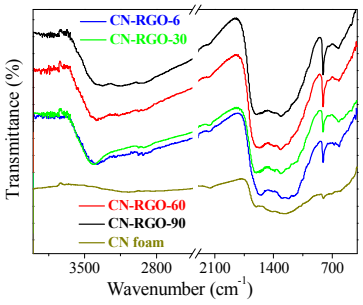


**Fig. 4** FT-IR spectra for CN foam and CN-RGO composites.

Raman spectroscopy is a powerful non-destructive tool for characterizing carbonaceous materials.[48] The typical Raman spectra of CN foam, CN-RGO-90, and graphite oxide are shown in Fig. SI-3 (see Supplementary Information). All of them show two prominent peaks, attributing to the typical D and G bands of carbon materials. The D band, observed at approximately 1351 $cm^{-1}$, is associated with the structural defects and disorders, while the G band, at about 1586 $cm^{-1}$, is usually found with graphitic structures and corresponds to the characteristic peak of C $sp^2$ atoms. This result further determines the formation of CN-RGO product.

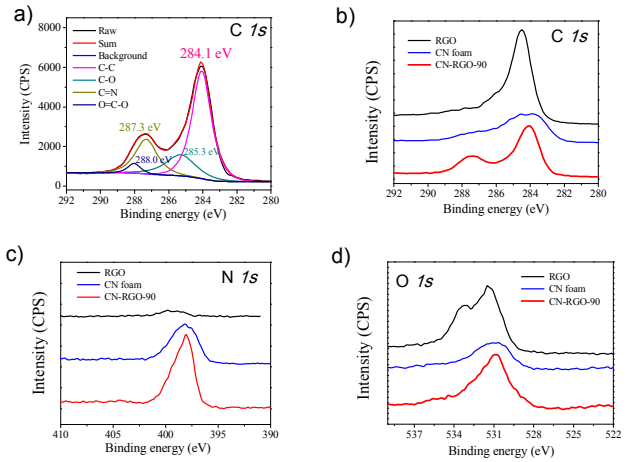


**Fig. 5** Detailed XPS spectra for a) C *1s* region of the CN-RGO-90; b) C *1s*, c) N *1s*, and d) O *1s* region for CN-RGO-90, pristine CN foam, and pure RGO obtained with annealing temperature of 300 °C.

X-ray photoelectron spectroscopy (XPS) was used to detect the element composition of the prepared CN-RGO monolith. The detailed XPS spectra for C, N and O elements of CN-RGO-90, pristine CN foam (prepared at 300 °C) and pure RGO (prepared at 300 °C) are shown in Fig. 5. Four obvious peaks detected in C 1s spectrum of CN-RGO-90 locate at 284.1, 285.3, 287.3 and 288.0 eV. The peak at 284.1 eV corresponds to C-C in aromatic rings, while the one at 287.3 eV can be assigned to C=N.[49, 50] The bands at 285.3 and 288.0 eV can be attributed to C-O (or C-N) and O=C–O (carbonates or carboxyl) groups, respectively.[51-53] Fig. 5b shows the comparison study of

C 1s spectra from CN-RGO-90, pristine CN foam, and pure RGO, which indicates that the peak at 287.3 eV (assigned to C=N) in CN-RGO-90 sample was mainly contributed by CN foam (Fig. SI-4, see Supplementary Information). In comparison with the C 1s spectra of graphite oxide in our previous study,[51] the peaks intensities of oxygen-containing groups in CN-RGO-90 sample decrease, indicating the partial removal of oxygen-containing functional groups.

From XPS analysis, the N content of the CN-RGO-90 product is 22.2 $_{atom.}$%. This value is comparable with the elemental analysis result (32.2 $_{atom.}$%). It can be seen that CN-RGO-90 sample and CN foam show quite similar peak in N 1s region (Fig. 5c), suggesting that nitrogen in the composite comes from CN foam. The deconvoluted spectra for N 1s in CN-RGO-90 sample show two binding energies at 397.9 and 399.0 eV, which can be indexed into pyridine-like nitrogen (C=N-C) and pyrrolic/pyridone-type N atoms, respectively (Fig. SI-5, see Supplementary Information).[54, 55] It is noteworthy that the pyridine-like nitrogen signal is higher than that of pyrrolic- and/or pyridone-type nitrogen, indicating the relatively higher concentration of the pyridine-like nitrogen in the product. The nitrogen composition would endow new or improved properties for the foam product.

As shown in Fig. 5d, oxygen element in the CN-RGO-90 product mainly comes from reduced graphene oxide. In the XPS spectrum of oxygen region (Fig. SI-6, see Supplementary Information), a peak at 530.9 eV would correspond to quinone, while the weak peaks at 532.8 and 533.4 eV would originate from the phenolic hydroxyl/ether and carboxyl, respectively. For the CN-RGO-90 product, the nitrogen/oxygen ratio was estimated to be 1:0.66 from XPS analysis. This is comparable with the elemental analysis result (1:0.43). The difference between them would indicate that the oxygen elemental richens on the surface of the product, since XPS spectrum analysis is a surface analysis technique.

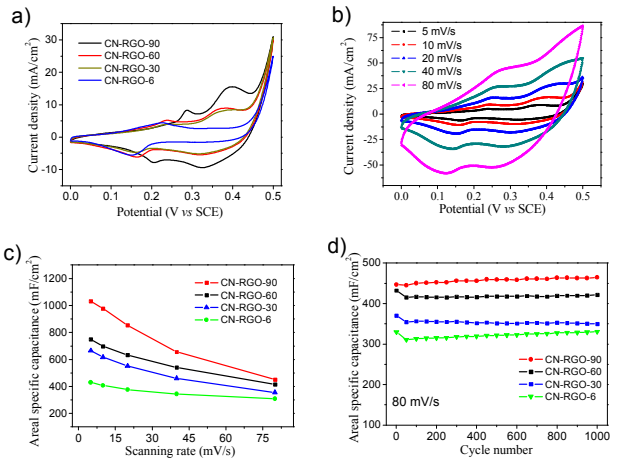


**Fig. 6** a) CV curves for different CN-RGO samples under the same scanning rate of 5 mV/s. b) CV curves for CN-RGO-60 product with scanning rates of 5, 10, 20, 40 and 80 mV/s. c) The specific capacitances calculated from CV curves under various scanning rates for all samples. d) Cycling performance tested through CV method for all samples.

Considering the unique porous microstructure, the monolith composite foams were then fabricated into supercapacitor electrode. The electrochemical performance of the integrated few-layer graphene/CN-nickel foam electrode was evaluated by CV and galvanostatic charge-discharge measurements. The composite foams with different RGO loading amounts were firstly compared.

Typical CV curves for the few-layer graphene/CN-nickel foam electrodes (corresponding to samples CN-RGO-90, CN-RGO-60, CN-RGO-30, and CN-RGO-6) between a potential window of 0 and 0.5 V (*vs* a saturated calomel electrode) at a scan rate of 5 mV/s are presented in Fig. 6a. It can be clearly observed that all of the tested CN-RGO/nickel foam electrodes exhibit wider CV curves, demonstrating their higher charge storage capability. Fig. 6b shows the CV curves of the CN-RGO-60 electrode with different scan rates (5-80 mV/s). Two pairs of prominent redox peaks can be clearly identified in the CV curves, which can be attributed to the nitrogen or oxygen composition in the foam.[56] This result clearly indicates pseudo-capacitance from the Faradaic processes contributes to the charge storage.[57] With the increase of scanning rates, the peak currents increased, suggesting that the materials are beneficial to fast redox reactions. The characteristic symmetry of the anodic and cathodic peaks at lower scanning rates indicates the electrochemical reversibility for the CN-RGO based electrode.

Fig. 6c shows the areal specific capacitances for various samples at different scanning rates. From CV results, the maximal areal specific capacitance of the CN-RGO/nickel foam electrode was calculated to be 1031 mF/cm$^2$ for CN-RGO-90 composite at scan rate of 5 mV/s. This is a relatively higher value for the reported supercapacitor materials in previous studies.[58-60] The areal capacitance of the CN-RGO/nickel foam electrodes decrease with the increase of scanning rates. This phenomenon is reasonable. At low scanning rates, the electrolytic ions can fully diffuse and migrate into active materials; while with high scanning rates, the diffusion effect limits the migration of the electrolytic ions and causes some active surface areas to become inaccessible for charge storage, thus inducing lower capacitance values. When the scanning rate increases from 5 to 80 mV/s, a capacitance retention rate of about 43.5-71.8% is achieved. In addition, from Fig. 6c, it can be seen that the higher areal specific capacitances are obtained with CN-RGO-90 and CN-RGO-60 electrodes. That is, with more RGO, higher specific capacitance values are obtained. This suggests that the charge storage of the composite electrodes is partially from RGO nanosheets.

Cycling stability is another important parameter for high-performance supercapacitors. Fig. 6d reveals the cycle performance of the CN-RGO/nickel foam electrodes measured with CV method at a scanning rate of 80 mV/s for 1000 cycles. After 1000 CV cycles, the electrodes show 94.5-104% specific capacitance of the initial value, indicating the excellent long-term stability of the electrodes.

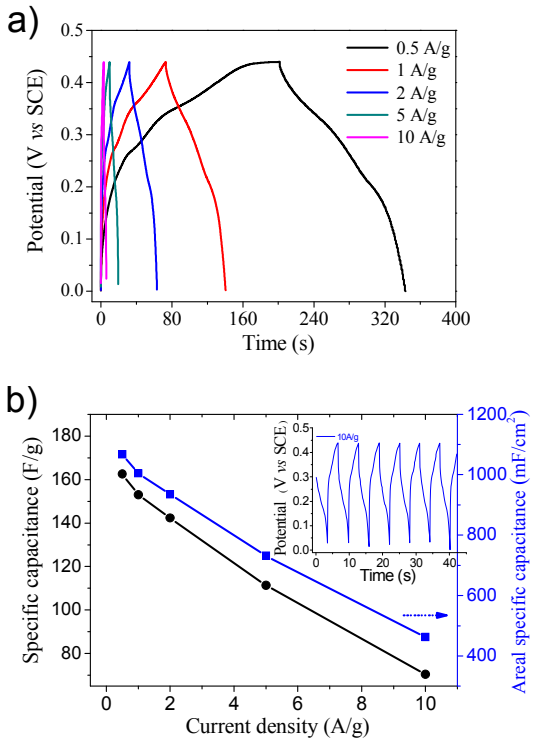


**Fig. 7** a) Galvanostatic charge-discharge curves for CN-RGO-90 electrode at various current densities (0.5-10 A/g) ; b) The corresponding galvanostatic specific capacitors of CN-RGO-90 as a function of the current densities.

To further evaluate the electrochemical properties and estimate the stable potential windows of the as-synthesized CN-RGO/nickel foam electrodes, galvanostatic charging and discharging of the fabricated electrode from CN-RGO-90 sample in 3 M KOH aqueous solution was performed. The charge-discharge curves at different current densities (0.5-10 A/g) between 0.0 and 0.44 V are displayed in Fig. 7a. Unlike the linear characteristic of electrochemical double layer capacitor electrodes, the charge/discharge curves of the CN-RGO/nickel foam electrode show two weak platforms, demonstrating pseudo-capacitance contribution, which substantiates the CV curve results.

The shown charge-discharge cycles in the inset of Fig. 7b at a current density of 10 A/g indicates stable reversible characteristics of the CN-RGO/nickel foam electrode. The specific capacitance of the CN-RGO-90 electrode can be further calculated from the discharge curves according to $C = (I\Delta t/m\Delta V)$ (F/g). Here $I$ is the discharge current ($A$), $\Delta t$ is the discharge time ($s$), $m$ is the mass of the active material in the electrode ($g$) and $\Delta V$ is the potential change during discharge ($V$). The specific capacitances obtained are 162, 153, 142, 111 and 70 F/g at current densities of 0.5, 1, 2, 5, and 10 A/g, respectively (Fig. 7b). The areal specific capacitance values can also be calculated from the above data, which give values of 1067, 1004, 934, 731 and 463 mF/cm$^2$ for different current densities. Clearly, the specific capacitance gradually decreases with increasing current density. In the tested current density range, the specific capacitance decreases to 43% of its initial value. It should be noted that our calculated mass of active materials includes the binder and the CN-RGO composites. These results confirm the relatively high specific capacitance values of the CN-RGO-based electrode.

**Table 1** Specific capacitance values obtained with various carbon materials.

| Carbon-based materials | Specific capacitance (F/g) | Current density (A/g) | Refs. |
|---|---|---|---|
| CN-RGO | [a]162 | 0.5 | this work |
| N-doped carbon spheres | 159 | 0.5 | (61) |
| Carbon from melamine resin | 23-132 | 0.25 | (40) |
| N-doped porous carbon from melamine | 37 | 0.02 | (38) |
| N-doped porous carbon from melamine | 204.8 | 0.02 | (37) |
| N-doped carbon electrodes | 153 | 0.5 | (62) |
| N-doped microporous carbon | 170-190 | 0.1 | (63) |
| N-doped carbon spheres from melamine | 192 | 0.1 | (64) |
| Graphene foam | ~70 | 0.5 | (65) |
| Graphene foam | ~50 | 0.1 | (58) |
| RGO-$MnO_2$ foam | ~125 | 1 | (31) |
| Ordered mesoporous carbons | ~210 | 0.5 | (66) |
| Carbon-coated graphene | 120 | 0.5 | (67) |
| Graphene/nitrogen-doped carbon | 189 | 0.1 | (68) |

[a] calculated based on mass of the binder and the CN-RGO

Table 1 shows the comparative results of various reported carbon-based materials for supercapacitors. The CN-RGO composite shown in this work exhibits a relatively high specific capacitance value, although proper comparison of the value is difficult because of the different test methods. The relative better performance would relate to its unique micro-/nanostructure. It is believed that it can also be further improved by optimization of test conditions, since it is not only affected by the materials' status (e.g. microstructure, size, etc) but also influenced by test conditions (such as electrolyte, current density, mass loading density, electrode system, and so on). [69]

It was found that integration of RGO and CN foam into composite monolith shows a strong enhancement effect on the charge storage performance. For comparison, electrodes fabricated from pristine CN foam and pure RGO obtained with annealing temperature of 300 $^{o}$C were tested in the same condition with galvanostatic charge-discharge methods. Fig. 8a shows the charge/discharge curves of the electrodes fabricated from CN-RGO-90, neat CN foam, and pure RGO at a current density of 0.5 A/g. The specific capacitances of pristine CN foam and pure RGO electrodes are 89 and 112 F/g at current densities of 0.5 A/g, respectively (Fig. 8a), which are quite smaller than that of CN-RGO-90 electrode (162 F/g). The areal specific capacitance values for the CN-RGO-90, neat CN foam, and pure RGO electrodes are 1067, 388 and 236 mF/cm$^2$ at current densities of 0.5 A/g, respectively (Fig. 8b), showing similar trend. These results confirm that both of CN foam and RGO nanosheets contribute to charge storage process and that integration of RGO and CN foam into composite monolith shows a strong enhancement effect on the electrochemical performance.

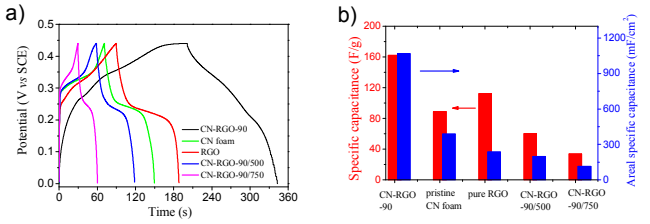


**Fig. 8** a) Galvanostatic charge-discharge curves and b) the corresponding specific capacitance values for CN-RGO-90, pristine CN foam (300 °C), pure RGO (300 °C), CN-RGO-90/500, and CN-RGO-90/750 electrodes tested under the same scanning rate of 0.5 A/g.

It is well known that the capacitance performance is highly influenced by electrode composition and its microstructure. The enhanced electrochemical performance of the CN-RGO composite can be attributed to the unique porous structure and the pseudocapacitive contribution from the nitrogen and oxygen composition. The prepared CN-RGO monoliths exhibit regular and interconnected macroporous architecture, which favors ions diffusion during charge storage process. Secondly, the few-layer graphene nanosheets loaded on the CN framework demonstrate free-standing state and provide rich accessible chemical sites for charge storage. In addition, the interconnected CN-RGO framework possesses excellent conductive paths, facilitating transport of electrons when it was used as capacitance electrode (Fig. SI-1, see Supplementary Information). Thus, the composite CN-RGO frameworks show better capacitance performance than that of pristine CN foam and pure RGO.

Annealing temperature in CN-RGO preparation process would also be an important influence factor for the electrochemical properties, since it would influence the conversion of graphene oxide to graphene and determine the oxygen and nitrogen content in the composite framework. To investigate the influence of annealing temperature, another two CN-RGO products, CN-RGO-90/500 and CN-RGO-90/750, were prepared and investigated (Fig. 8a-b). The results indicate that the CN-RGO monolith prepared at 300 °C shows the best charge storage ability among the tested three samples. At current density of 0.5 A/g, the specific capacitance values of CN-RGO-90/500 and CN-RGO-90/750 obtained from galvanostatic charge-discharge curves are 60 F/g (200 mF/cm$^2$) and 34 F/g (113 mF/cm$^2$) (Fig. 8a-b). Both of them are smaller than that of CN-RGO-90 prepared at 300 °C. It can be seen that with the increasing of annealing temperature, the specific capacitance values gradually decrease. Increasing of annealing temperature will induce the decrease of oxygen content in graphene oxide and favor full conversion of graphene oxide to graphene, and so inducing the increase of electrical conductivity. While, at the same time, higher annealing temperature will cause the loss of nitrogen in the CN framework. The relative low nitrogen and oxygen content in the monoliths will decrease their pseudocapacitive contribution. It seems that in our case the latter gives a main influence for the charge storage performance. Thus, the specific capacitance values gradually decrease with the increasing of annealing temperature.

## Conclusions

In summary, we have demonstrated a simple method for loading few-layer RGO sheets on CN foam, forming a unique hierarchical structured monolith. The composite monolith can be cut into various shapes and sizes. The loading density of RGO on CN foam can be tuned by the dosage of GO. This method for CN-RGO foam can be scalable. The obtained composite foam was then fabricated as electrodes for supercapacitors. The free-standing, light-weight, and conductive monoliths present excellent electrochemical charge storage ability with high stability. The unique microstructure and nitrogen/oxygen composition in the CN framework is believed to contribute to the excellent charge storage ability. The monolith CN-RGO foam would be further used as a promise substrate for loading various functional materials used in electrochemical fields.

## Acknowledgements

The authors are grateful for financial support from National Natural Science Foundation of China (No. 51102117, 51203069, 51272094), Jiangsu Natural Science Foundation (No. BK2012276), and Cultivating Project of Young Academic Leader from Jiangsu University.

## Notes and references

[a] School of Chemistry and Chemical Engineering, Jiangsu University, Zhenjiang, 212013, P. R. China, Fax:(+86)511-88791800; Tel:(+86)511-88791800; E-mail: zhuguoxing@ujs.edu.cn; xiaopingshen@163.com
[b] School of Environmental and Chemical Engineering, Jiangsu University of Science and Technology, Zhenjiang 212013, P. R. China.
[c] State Key Laboratory of Coordination Chemistry, Nanjing National Laboratory of Microstructures, Nanjing University, Nanjing, 210093, P. R. China.

† Electronic Supplementary Information (ESI) available: [FT-IR, XPS, and Raman spectra, electrical conductivity measurement, table showing element analysis result]. See DOI: 10.1039/b000000x/

1 H. Jiang, J. Ma and C. Z. Li, *Adv. Mater.*, 2012, **24**, 4197-4202.
2 M. E. Plonska-Brzezinska and L. Echegoyen, *J. Mater. Chem. A*, 2013, **1**, 13703-13714.
3 J. Yang, P. X. Xiong, C. Zheng, H. Y. Qiu and M. D. Wei, *J. Mater. Chem. A*, 2014, **2**, 16640-16644.
4 G. X. Zhu, C. Y. Xi, M. Q. Shen, C. L. Bao and J. Zhu, *ACS Appl. Mater. Interfaces*, 2014, **6**, 17208-17214.
5 G. Lota, K. Fic and E. Frackowiak, *Energy Environ. Sci.*, 2011, **4**, 1592-1605.
6 L. F. Wang, S. Lin, K. F. Lin, C. Y. Yin, D. S. Liang, Y. Di, P. W. Fan, D. Z. Jiang and F. S. Xiao, *Microp. Mesop. Mater.*, 2005, **85**, 136-142.

7 J. Zhi, W. Zhao, X. Y. Liu, A. R. Chen, Z. Q. Liu and F. Q. Huang, *Adv. Funct. Mater.*, 2014, **24**, 2013-2019.
8 X. Y. Chen, C. Chen, Z. J. Zhang and D. H. Xie, *J. Mater. Chem. A*, 2013, **1**, 7379-7383.
9 H. Pang, Q. Y. Lu and F. Gao, *Chem. Commun.*, 2011, **47**, 11772-11774.
10 A. Kurniawan, L. K. Ong, F. Kurniawan, C. X. Lin, F. E. Soetaredjo, X. S. Zhao and S. Ismadji, *RSC Adv.*, 2014, **4**, 34739-34750.
11 D. Y. Qu and H. Shi, *J. Power Sources*, 1998, **74**, 99-107.
12 M. S. Balathanigaimani, W. G. Shim, M. J. Lee, C. Kim, J. W. Lee and H. Moon, *Electrochem. Commun.*, 2008, **10**, 868-871.
13 V. Ruiz, C. Blanco, R. Santamaria, J. M. Ramos-Fernandez, M. Martinez-Escandell, A. Sepulveda-Escribano and F. Rodriguez-Reinoso, *Carbon*, 2009, **47**, 195-200.
14 K. H. An, W. S. Kim, Y. S. Park, J. M. Moon, D. J. Bae, S. C. Lim, Y. S. Lee and Y. H. Lee, *Adv. Funct. Mater.*, 2001, **11**, 387-392.
15 C. M. Yang, Y. J. Kim, M. Endo, H. Kanoh, M. Yudasaka, S. Iijima and K. Kaneko, *J. Am. Chem. Soc*., 2006, **129**, 20-21.
16 L. B. Hu, J. W. Choi, Y. Yang, S. Jeong, F. L. Mantia, L. F. Cui and Y. Cui, *Proc. Natl. Acad. Sci. U.S.A.*, 2009, **106**, 21490-21494.
17 Y. Q. Sun, Q. Wu and G. Q. Shi, *Energy Environ. Sci.*, 2011, **4**, 1113-1132.
18 S. J. Li, D. H. Deng, H. Pang, L. Liu, Y. Xing and S. R. Liu, *J. Solid State Electrochem.*, 2012, **16**, 2883-2889.
19 Y. W. Zhu, S. Murali, M. D. Stoller, K. J. Ganesh, W. W. Cai, P. J. Ferreira, A. Pirkle, R. M. Wallace, K. A. Cychosz, M. Thommes, D. Su, E. A. Stach and R. S. Ruoff, *Science*, 2011, **332**, 1537-1541.
20 C. G. Liu, Z. N. Yu, D. Neff, A. Zhamu and B. Z. Jang, *Nano Lett.*, 2010, **10**, 4863-4868.
21 Y. M. Tan, C. F. Xu, G. X. Chen, Z. H. Liu, M. Ma, Q. J. Xie, N. F. Zheng and S. Z. Yao, *ACS Appl. Mater. Interfaces*, 2013, **5**, 2241-2248.
22 H. Y. Liu, K. P. Wang and H. Teng, *Carbon*, 2005, **43**, 559-566.
23 M. M. Titirici, R. J. White, N. Brun, V. L. Budarin, D. S. Su, F. D. Monte, J. H. Clark and M. J. MacLachlan, *Chem. Soc. Rev.*, 2015, **44**, 250-290.
24 E. Frackowiak and F. Béguin, *Carbon*, 2001, **39**, 937-950.
25 H. Nishihara and T. Kyotani, *Adv. Mater.*, 2012, **24**, 4473-4498.
26 B. G. Choi, M. Yang, W. H. Hong, J. W. Choi and Y. S. Huh, *ACS Nano*, 2012, **6**, 4020-4028.
27 B. You, J. H. Jiang and S. J. Fan, *ACS Appl. Mater. Interfaces*, 2014, **6**, 15302-15308.
28 X. L. Fang, J. Zang, X. L. Wang, M. S. Zheng and N. F. Zheng, *J. Mater. Chem. A*, 2014, **2**, 6191-6197.
29 S. B. Ye and J. C. Feng, *ACS Appl. Mater. Interfaces*, 2014, **6**, 9671-9679.
30 X. C. Zhao, Q. Zhang, C. M. Chen, B. S. Zhang , S. Reiche, A. Q. Wang, T. Zhang, R. Schlogl and D. S. Su, *Nano Energy*, 2012, **1**, 624-630.
31 J. Ge, H. B. Yao, W. Hu, X. F. Yu, Y. X. Yan, L. B. Mao, H. H. Li, S. S. Li and S. H. Yu, *Nano Energy*, 2013, **2**, 505-513.
32 D. Hulicova, J. Yamashita, Y. Soneda, H. Hatori and M. Kodama, *Chem. Mater.*, 2005, **17**, 1241-1247.
33 D. Hulicova, M. Kodama and H. Hatori, *Chem. Mater.*, 2006, **18**, 2318-2326.
34 S. Dutta, A. Bhaumik and K. C. Wu, *Energy Environ. Sci.*, 2014, **7**, 3574-3592.
35 E. Fiset, T. E. Rufford, M. Seredych, T. J. Bandosz, D. Hulicova-Jurcakova, *Carbon*, 2015, **81**, 239-250.
36 S. L. Chen, G. H. He, H. Hu, S. Q. Jin, Y. Zhou, Y. Y. He, S. J. He, F. Zhao and H. Q. Hou, *Energy Environ. Sci.*, 2013, **6**, 2435-2439.
37 C. L. Qin, X. Lu, G. P. Yin, Z. Jin, Q. Tan and X. D. Bai, *Mater. Chem. Phys.*, 2011, **126**, 453-458.
38 W. Z. Shen and W. B. Fan, *J. Mater. Chem. A*, 2013, **1**, 999-1013.
39 M. Li and J. M. Xue, *J. Phys. Chem. C*, 2014, **118**, 2507-2517.
40 U. B. Nasini, V. G. Bairi, S. K. Ramasahayam, S. E. Bourdo, T. Viswanathan and A. U. Shaikh, *J. Power Sources*, 2014, **250**, 257-265.
41 R. M. Li, A. M. Cao, Y. J. Zhang, G. Li, F. Jiang, S. M. Li, D. Q. Chen, C. R. Wang, J. C. Ge and C. Y. Shu, *ACS Appl. Mater. Interfaces*, 2014, **6**, 20574-20578.
42 W. S. Hummers and R. E. Offeman, *J. Am. Chem. Soc.*, 1958, **80**, 1339-1339.
43 C. Zhang, W. Lv, X. Y. Xie, D. M. Tang, C. Liu and Q. H. Yang, *Carbon*, 2013, **62**, 11-24.
44 M. J. McAllister, J. L. Li, D. H. Adamson, H. C. Schniepp, A. A. Abdala, J. Liu, M. Herrera-Alonso, D. L. Milius, R. Car, R. K. Prud'homme and I. A. Aksay, *Chem Mater*, 2007, **19**, 4396-4404.
45 W. Lv, D. M. Tang, Y. B. He, C. H. You, Z. Q. Shi, X. C. Chen, C. M. Chen, P. X. Hou, C. Liu and Q. H. Yang, *ACS Nano*, 2009, **3**, 3730-3736.
46 M. J. Allen, V. C. Tung and R. B. Kaner, *Chem. Rev.*, 2010, **110**, 132-145.
47 F. Dong, L. W. Wu, Y. J. Sun, M. Fu, Z. B. Wu and S. C. Lee, *J. Mater. Chem.*, 2011, **21**, 15171-15174.
48 A. M. Rao, E. Richter, S. J. Bandow, B. Chase, P. C. Eklund, K. A. Williams, S. Fang, K. R. Subbaswamy, M. Menon, A. Thess, R. E. Smalley, G. Dresselhaus and M. S. Dresselhaus, *Science*, 1997, **275**, 187-191.
49 Ishpal, O. S. Panwar, M. Kumar and S. Kumar, *Appl. Surf. Sci.*, 2010, **256**, 7371-7376.
50 L. Qie, W. M. Chen, H. H. Xu, X. Q. Xiong, Y. Jiang, F. Zou, X. L. Hu, Y. Xin, Z. L. Zhang and Y. H. Huang, *Energy Environ. Sci.*, 2013, **6**, 2497-2504.
51 S. Bai, X. P. Shen, G. X. Zhu, A. H. Yuan, J. Zhang, Z. Y. Ji and D. Z. Qiu, *Carbon*, 2013, **60**, 157-168.
52 R. Gokhale, V. Aravindan, P. Yadav, S. Jain, D. Phase, S. Madhavi, S. Ogale, *Carbon*, 2014, **80**, 462-471.
53 H. H. Zhang, Q. Liu, K. Feng, B. Chen, C. H. Tung and L. Z. Wu, *Langmuir*, 2012, **28**, 8224-8229.
54 L. Hao, B. Luo, X. L. Li, M. H. Jin, Y. Fang, Z. H. Tang, Y. Y. Jia, M. H. Liang, A. Thomas, J. H. Yang and L. J. Zhi, *Energy Environ. Sci.*, 2012, **5**, 9747-9751.
55 L. Sun, C. G. Tian, Y. Fu, Y. Yang, J. Yin, L. Wang and H. G. Fu, *Chem. Eur. J.*, 2014, **20**, 564-574.
56 J. T. Zhang, J. Wang, J. Yang, Y. L. Wang and M. B. Chan-Park, *ACS Sustain. Chem. Eng.*, 2014, **2**, 2291-2296.
57 X. W. Mao, G. C. Rutledge and T. A. Hatton, *Nano Today*, 2014, **9**, 405-432.
58 Z. Y. Yang, L. J. Jin, G. Q. Lu, Q. Q. Xiao, Y. X. Zhang, L. Jing, X. X. Zhang, Y. M. Yan and K. N. Sun, *Adv. Funct. Mater.*, 2014, **24**, 3917-3925.

59 R. Vellacheri, A. Al-Haddad, H. P. Zhao, W. X. Wang, C. L. Wang and Y. Lei, *Nano Energy*, 2014, **8**, 231-237.
60 Q. H. Ji, X. Zhao, H. J. Liu, L. Guo and J. H. Qu, *ACS Appl. Mater. Interfaces*, 2014, **6**, 9496-9502.
61 W. R. Li, D. H. Chen, Z. Li, Y. F. Shi, Y. Wan, G. Wang, Z. Y. Jiang and D. Y. Zhao, *Carbon*, 2007, **45**, 1757-1763.
62 D. Hulicova-Jurcakova, M. Kodama, S. Shiraishi, H. Hatori, Z. H. Zhu and G. Q. Lu, *Adv. Funct. Mater.*, 2009, **19**, 1800-1809.
63 A. B. Fuertes, G. A. Ferrero and M. Sevilla, *J. Mater. Chem. A*, 2014, **2**, 14439-14448.
64 W. H. Lee and J. H. Moon, *ACS Appl. Mater. Interfaces*, 2014, **6**, 13968-13976.
65 Z. W. Xu, Z. Li, C. M. B. Holt, X. H. Tan, H. L. Wang, B. S. Amirkhiz, T. Stephenson and D. Mitlin, *J. Phys. Chem. Lett.*, 2012, **3**, 2928-2933.
66 S. P. Wang, C. L. Han, J. Wang, J. Deng, M. L. Zhu, J. Yao, H. R. Li and Y. Wang, *Chem. Mater.*, 2014, **26**, 6872-6877.
67 K. S. Kim and S. J. Park, *Electrochim. Acta*, 2011, **56**, 6547-6553.
68 M. Zhou, F. Pu, H. Chen, Z. Wang, H. Y. Zhang and S. Y. Guan, *New J. Chem.*, 2013, **37**, 4148-4155.
69 G. P. Wang, L. Zhang, J. J. Zhang, *Chem. Soc. Rev.*, 2012, **42**, 797-828.

# Table of Contents Entry

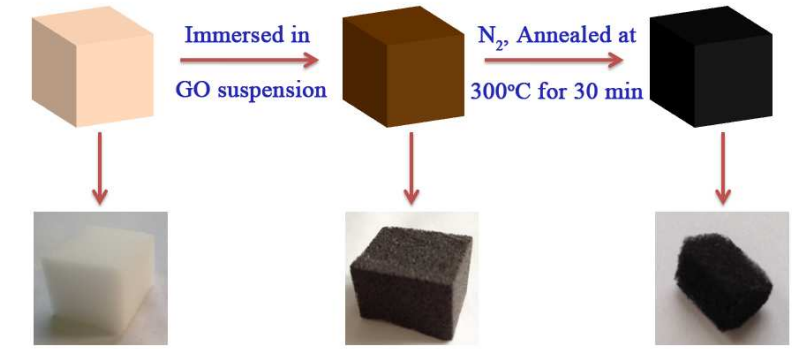


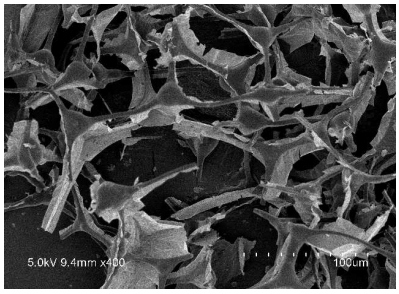


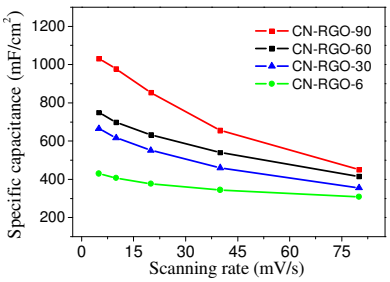


CN-RGO composite with excellent capacitive performance was prepared through a facile and rapid two-step strategy.